

Article

Investigation on Influencing Mechanism of Processing Parameters on Corrosion Resistance and Zinc Content of Anodic Coatings Developed on Magnesium Alloys in Near-Neutral Solutions

Wenxia Zhang ^{1,†}, Yuanyuan Zhu ^{1,2,†}, Rongfang Zhao ¹, Shufang Zhang ¹, Xinying Lai ¹, Yibo Wang ¹, Zekun Yan ¹, Wenjing Liu ¹ and Rongfa Zhang ^{1,*} 

¹ School of Materials and Electromechanics, Jiangxi Science and Technology Normal University, Nanchang 330013, China

² R & D Department, Zhejiang Ruigu Biotechnology Co., Ltd., Hangzhou 311121, China

* Correspondence: rfzhang-10@163.com

† Co-first author.

Abstract: In near-neutral solutions, the effects of NH_4HF_2 , H_3PO_4 , phytic acid (IP6), and EDTA-ZnNa₂ concentration on corrosion resistance and the Zn amount of micro-arc oxidation (MAO) coatings were revealed by an orthogonal experiment. The influencing order of four factors on coating corrosion resistance is EDTA-ZnNa₂ > NH_4HF_2 > IP6 > H_3PO_4 , while the sequence on the Zn amount is ranked as EDTA-ZnNa₂ > NH_4HF_2 > H_3PO_4 > IP6. The fabricated Zn-containing coatings exhibit excellent corrosion resistance, and their i_{corr} values are two orders of magnitude lower than that of the WE43 substrate, while the highest Zn amount achieves 4.12 wt.%. P and F compete to take part in coating formation, and Zn ions enter into anodic coatings by diffusion. Coating corrosion resistance is jointly determined by surface characteristics, which will provide the important theoretical foundation for fabricating Zn-containing coating with high corrosion resistance.

Keywords: corrosion resistance; magnesium alloys; micro-arc oxidation; influencing mechanism; zinc amount



Citation: Zhang, W.; Zhu, Y.; Zhao, R.; Zhang, S.; Lai, X.; Wang, Y.; Yan, Z.; Liu, W.; Zhang, R. Investigation on Influencing Mechanism of Processing Parameters on Corrosion Resistance and Zinc Content of Anodic Coatings Developed on Magnesium Alloys in Near-Neutral Solutions. *Coatings* **2022**, *12*, 1286. <https://doi.org/10.3390/coatings12091286>

Academic Editor: Alina Vladescu

Received: 6 August 2022

Accepted: 27 August 2022

Published: 2 September 2022

Publisher's Note: MDPI stays neutral with regard to jurisdictional claims in published maps and institutional affiliations.



Copyright: © 2022 by the authors. Licensee MDPI, Basel, Switzerland. This article is an open access article distributed under the terms and conditions of the Creative Commons Attribution (CC BY) license (<https://creativecommons.org/licenses/by/4.0/>).

1. Introduction

Compared with traditional bone-repair materials such as titanium alloys, stainless steel, and cobalt-based alloys [1], magnesium (Mg) alloys have been thought to be excellent materials for metallic implants due to their similar density to natural bone and good biodegradability in bioenvironment [2]. However, Mg alloys belong to very active metals with a too-fast corrosion rate in vivo, which may cause surgery failure [3]. Therefore, it is necessary to improve corrosion resistance of Mg alloys to meet clinical applications [4].

Various technologies, such as purification, alloying, and surface treatment, have been developed to improve corrosion resistance of Mg alloys [2,5]. Among these surface treatment methods, micro-arc oxidation (MAO) can effectively develop ceramic coatings with thick, hard, and adherent properties on aluminum alloys [6,7] and Mg alloys [8–13]. The coating components are especially easily manipulated by selecting the electrolyte composition and concentration [8–10] and electrical parameters [11]. Recently, MAO coatings have been functionalized by doping an appropriate amount of zinc (Zn) element [14–16]. As an important trace element, Zn distributes in all tissues and organs and participates in many enzymatic reactions [17]. It is reported that Zn plays an important role in bone metabolism, cell metabolism and apoptosis, gene expression, and neurotransmission [18]. Zn is also closely related with human intelligence, memory, and neurological disorders such as cerebral ischemia and Alzheimer's disease. Moreover, zinc has a positive effect on improving immunity [19]. In addition to directly promote the development and function

of immune organs, Zn can also directly act on certain bacteria and viruses and possesses strong antibacterial properties [20]. Therefore, it is important to fabricate Zn-containing coatings on medical Mg alloys.

For Mg alloys, MAO coatings are generally fabricated in strong alkaline solutions containing silicate [14], phosphate [21], and natural organic phytic acid ($C_6H_6(H_2PO_4)_6$, abbreviated as IP6 [22]). At present, Zn-doped MAO coatings on Mg alloys are rarely reported using a one-step method [23], and the reported coatings were developed in strong alkaline solutions [14–16]. Compared with alkaline solutions, near-neutral solutions cannot only achieve a higher final voltage and therefore better surface property, but also prolong solution service lifetime [22]. In this study, ammonium bifluoride (NH_4HF_2), phosphoric acid (H_3PO_4), IP6, and ethylene diamine tetraacetic acid zinc disodium salt ($(NaOOCCH_2)_2-N=CH_2CH_2=N(CH_2COO)_2Zn$, abbreviated as EDTA-ZnNa₂) were selected as MAO electrolytes to develop ceramic coatings on WE43 substrate in a near-neutral solution composed of 360 g/L hexamethylenetetramine (HMTA). The influencing regularity of electrolyte composition and concentration on coating property were clarified by using an orthogonal experiment. More specifically, NH_4HF_2 was used as a corrosive inhibitor of Mg alloys, while EDTA-ZnNa₂ was used as a Zn-containing electrolyte. H_3PO_4 and IP6 were selected as inorganic and organic P-containing electrolytes, respectively. The prepared anodic coatings were measured by SEM (Σ IGMA, Zeiss Sigma, Oberkochen, Germany), XRD (Shimadzu XRD-6100, Kyoto, Japan), XPS (ESCALAB250, Thermo VG, Waltham, MA, USA), and potentiodynamic polarization curves to clarify the affecting regularity of electrolyte composition and concentration on coating corrosion resistance and the Zn content.

2. Experimental

2.1. Materials and Coating Preparation

Extruded WE43 provided from Suzhou Chuan Mao Metal Materials Co., LTD (Suzhou, China), contained 4.01 wt.% Y, 0.47 wt.% Zr, 1.72 wt.% Gd, 2.35 wt.% Nd, 0.003 wt.% Cu, 0.004 wt.% Ni, 0.0003 wt.% Fe, and balanced Mg. Before MAO treatment, all samples were first ground by using SiC waterproof abrasive paper and then cleaned successively with distilled water and ethyl alcohol. Finally, all samples were dried by using a hairdryer. The selected base solution in this study was composed of 360 g/L HMTA (Ph = 6.30). According to Table 1, the effects of NH_4HF_2 , H_3PO_4 , IP6, and EDTA-ZnNa₂ concentration on corrosion resistance and the Zn amount were investigated via an orthogonal experiment with four factors and three levels.

Table 1. Experimental arrangement and results detailing concentration effects of NH_4HF_2 , H_3PO_4 , IP6, and EDTA-ZnNa₂ on sample i_{corr} and Zn content.

Process No.	NH_4HF_2 (g/L)	H_3PO_4 (g/L)	IP6 (g/L)	EDTA-ZnNa ₂ (g/L)	i_{corr} ($\times 10^{-8} A \cdot cm^{-2}$)	Zn Content (wt.%)
No. 1	3	15	4	6	11.20	2.03
No. 2	3	25	8	10	3.26	3.20
No. 3	3	35	12	14	7.01	4.12
No. 4	6	15	8	14	10.88	2.94
No. 5	6	25	12	6	8.56	1.44
No. 6	6	35	4	10	7.39	2.71
No. 7	9	15	12	10	1.09	1.48
No. 8	9	25	4	14	6.18	2.35
No. 9	9	35	8	6	8.06	1.42
K1	21.47 (9.35)	23.17 (6.45)	24.77 (7.09)	27.82 (4.89)	-	-
K2	26.83 (7.09)	18.00 (6.99)	22.20 (7.56)	11.74 (7.39)	-	-
K3	15.33 (5.25)	22.46 (8.25)	16.66 (7.04)	24.07 (9.41)	-	-
Difference	11.50 (4.10)	5.17 (1.80)	8.11 (0.52)	16.08 (4.52)	-	-
Rank	2 (2)	4 (3)	3 (4)	1 (1)	-	-

According to the processing conditions given in Table 1, nine MAO samples, namely No. 1 to No. 9, were prepared by using a homemade MAO-5D power supply (Chengdu Tongchuang New Material Surface Engineering and Technology Center, Chengdu, China). A WE43 sample was used as the anode, while a stainless-steel barrel with the MAO solution was connected with the cathode. By adopting a constant current control mode, the selected current density, duty cycle, frequency, and treating time were 60 mA/cm², 35%, 2000 Hz, and 3 min, respectively. The solution pH was determined by using a PHS-3C digital pH meter (Shanghai Yoke Instrument Co., Ltd., Shanghai, China). The MAO solution was continually stirred to ensure its temperature under 40 °C.

2.2. Microstructural Characterization

Surface and cross-sectional morphologies were measured by a field emission scanning electron microscope (FE-SEM). Coating compositions were detected by an energy-dispersive X-ray spectrometer (EDS, OxfordINCA Energy, Oxford, UK) attached to an FE-SEM. In the 2 θ range of 10° to 80°, at a scanning speed of 4°/min, coating phase structures were analyzed by an X-ray diffractometer, using a Cu K α radiation. Chemical states of anodic coatings were detected by an X-ray photoelectron spectroscopy (XPS), with an Al K α anode ($\lambda = 1486.6$ eV). The porosity of MAO coatings was detected by Image-Pro Plus 6.0 imaging software.

2.3. Electrochemical Test

In order to evaluate the corrosion resistance of the WE43 substrate and MAO-treated samples, potentiodynamic polarization curves were measured by an electrochemical workstation (Reference 600+, Gamry Instruments, Lafayette, LA, USA). All measurements were performed at 37 °C in Hanks' solutions, as reported by others [22]. A typical three-electrode cell was used with a sample as the working electrode, while a saturated calomel electrode (SCE) (Tianjin Aida Hengsheng Technology Development Co., Ltd, Tianjin, China) and a platinum electrode were separately served as the reference electrode and the counter electrode, respectively. The initial delay and scanning rate were set as 300 s and 1 mV/s, respectively. Potentiodynamic polarization curves were measured from -0.25 to 0.5 V with respect to the open circuit potential (OCP), and the Tafel extrapolation method was used to derive the corresponding electrochemical parameters, including corrosion potential (E_{corr}), corrosion current density (i_{corr}), and anodic/cathodic Tafel slopes [24,25]. In order to ensure result repeatability, five parallel samples were measured to obtain the final results.

3. Results

3.1. Coating Surface Characteristics

3.1.1. Surface Morphology and Composition

As shown in Figure 1, it was evident that MAO coatings fabricated by nine processes displayed typically porous characteristics due to spark discharge (Figure 1a–i). Anodic coatings developed on samples No. 4, No. 7, and No. 8 exhibited uniform characteristics, with pore sizes in the range of 1 to 4 μm (Figure 1d,g,h), while most micropores on samples No. 5 and No. 9 (especially No. 9) were larger than 5 μm in diameter (Figure 1i). According to EDS spectra, anodic coatings developed on nine samples were mainly composed of C, O, F, Na, Mg, P, and Zn elements (Figure 2). It was clear that the coating compositions were closely related with processing parameters. Sample No. 3 achieved the highest Zn amount, i.e., 4.12 wt.%, while sample No. 9 had the lowest Zn amount, i.e., 1.42 wt.% (Figure 2i).

3.1.2. Cross-Sectional Morphology

According to the cross-sectional morphologies shown in Figure 3, samples No. 4 and No. 8 exhibited a comparatively uniform and porous microstructure (Figure 3d,h), while many micropores were developed on other samples, especially sample No. 9. The thicknesses of anodic coatings developed on samples Nos. 1–9 were 12.89 ± 0.63 , 16.06 ± 1.31 , 20.31 ± 1.60 , 11.30 ± 0.78 , 15.26 ± 0.82 , 10.41 ± 0.69 , 8.92 ± 0.10 , 10.49 ± 0.46 , and

$11.69 \pm 0.70 \mu\text{m}$ (Figure 3a–i), respectively. Among these samples, the anodic coating on samples No. 3 was the thickest, i.e., $20.31 \pm 1.60 \mu\text{m}$. However, sample No. 7 achieved the thinnest coating, only $8.92 \pm 0.10 \mu\text{m}$ (Figure 3g).

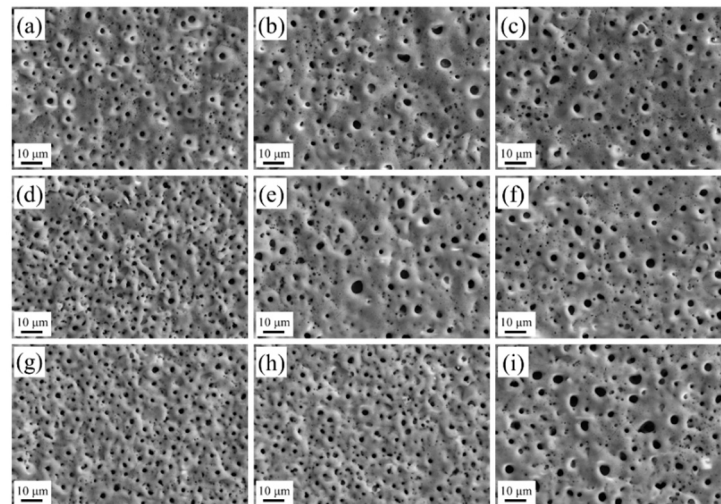


Figure 1. Surface morphologies of MAO coatings fabricated by nine processes: (a) No. 1, (b) No. 2, (c) No. 3, (d) No. 4, (e) No. 5, (f) No. 6, (g) No. 7, (h) No. 8, and (i) No. 9.

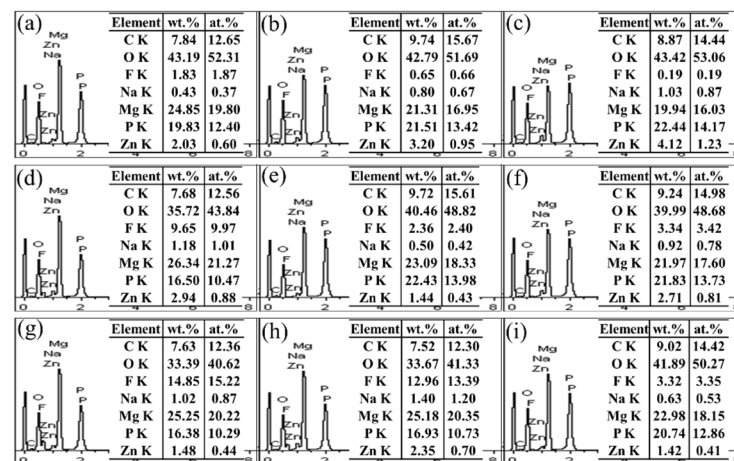


Figure 2. EDS spectra and chemical compositions of MAO coatings fabricated by nine processes: (a) No. 1, (b) No. 2, (c) No. 3, (d) No. 4, (e) No. 5, (f) No. 6, (g) No. 7, (h) No. 8, and (i) No. 9.

3.1.3. XRD Analysis

According to Figure 2, the Zn amounts on No. 3, No. 4, No. 5, and No. 7 were 4.12, 2.94 wt.%, 1.44 wt.%, and 1.48 wt.%, respectively. The XRD spectra of the four MAO samples mentioned above are displayed in Figure 4. Anodic coatings mainly contained Mg phase and MgO, while P-containing or F-containing crystalline components were not found, indicating that these substances existed mainly in amorphous state. The diffraction peaks of the WE43 substrate were detected, and they could be attributed to thin and porous MAO coatings.

3.1.4. XPS Analysis

An XPS analysis was used to clarify elemental chemical states of sample No. 4. The developed anodic coatings were mainly composed of Mg, Na, P, C, O, F, and Zn elements (Figure 5a). The C 1s spectrum exhibited two peaks at 284.6 and 285.4 eV (Figure 5b), corresponding to C-C(H) and C-O, respectively [26]. As shown in Figure 5c, the P 2p spectrum was fitted into two peaks, at 133.6 and 134.4 eV, assigned to PO_4^{3-} and HPO_4^{2-} ,

respectively [27]. The Zn 2p spectrum was fitted into two peaks located at 1023.5 and 1046.8 eV (Figure 5d), assigned to $Zn_3(PO_4)_2$ [14,28]. The F 1s spectrum exhibited only one peak at 686.3 eV (Figure 5e), which was ascribed to MgF_2 [29]. Mg 1s spectrum was decomposed into four peaks (Figure 5f), which were separately assigned to MgO, $Mg_3(PO_4)_2$, $MgHPO_4$, and MgF_2 .

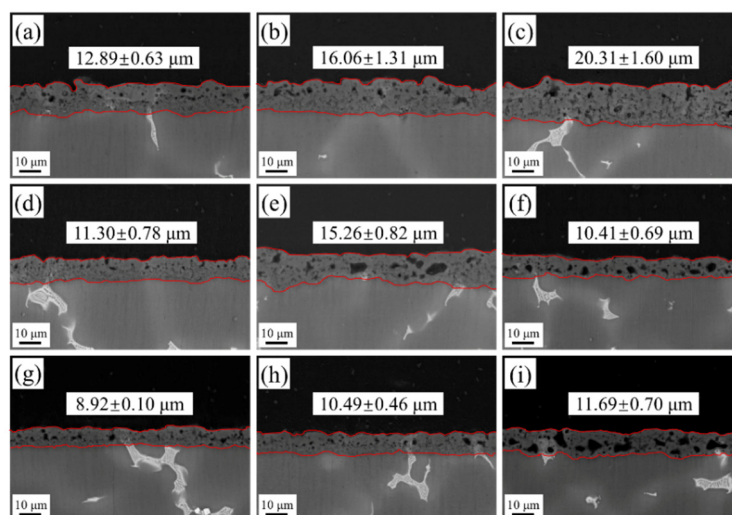


Figure 3. Cross-sectional morphologies of MAO coatings fabricated by nine processes: (a) No. 1, (b) No. 2, (c) No. 3, (d) No. 4, (e) No. 5, (f) No. 6, (g) No. 7, (h) No. 8, and (i) No. 9.

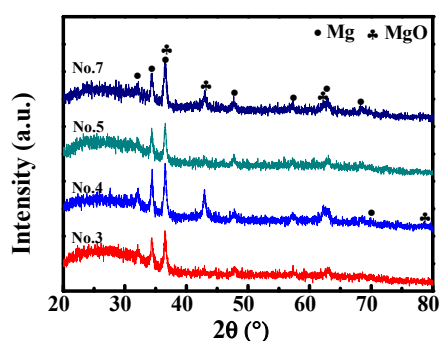


Figure 4. Coating XRD patterns formed on samples No. 3, No. 4, No. 5, and No. 7.

3.1.5. Coating Corrosion Resistance

Potentiodynamic polarization curves of WE43 substrate and nine MAO samples are shown in Figure 6. The fitted i_{corr} values using Gamry's software are listed in Table 2. Surface-treated samples achieved lower i_{corr} values and, therefore, have better corrosion resistance than the WE43 substrate. As listed in Table 2, sample No. 7 achieved the lowest i_{corr} value ($1.09 \times 10^{-8} \text{ A}\cdot\text{cm}^{-2}$), which was three orders of magnitude lower than that of the WE43 substrate ($2.11 \times 10^{-5} \text{ A}\cdot\text{cm}^{-2}$). The i_{corr} values of samples No. 1 and No. 4 were separately 1.12×10^{-7} and $1.09 \times 10^{-7} \text{ A}\cdot\text{cm}^{-2}$, two orders of magnitude lower than that of the WE43 substrate.

3.2. The Orthogonal Results

In this study, the measured i_{corr} and Zn amounts were selected as the objective parameters, and the experimental results were obtained by using the intuitionistic analysis. Based on the values of the differences listed in Table 1, the influencing order of four factors on i_{corr} of MAO samples was $\text{EDTA-ZnNa}_2 > \text{NH}_4\text{HF}_2 > \text{IP6} > \text{H}_3\text{PO}_4$. In detail, EDTA-ZnNa_2 was the first important factor influencing coating corrosion resistance. With the increasing EDTA-ZnNa_2 concentration, i_{corr} values decreased from Level 1 to Level 2 but increased

from Level 2 to Level 3, showing that a proper EDTA-ZnNa₂ concentration was helpful for improving corrosion resistance. For increasing NH₄HF₂ concentration, i_{CORR} values slightly increased from Level 1 to Level 2 but significantly decreased from Level 2 to Level 3. The IP6 concentration was the third important factor influencing the i_{CORR} value, and with the increase of IP6 concentration, i_{CORR} values gradually decreased (Table 1).

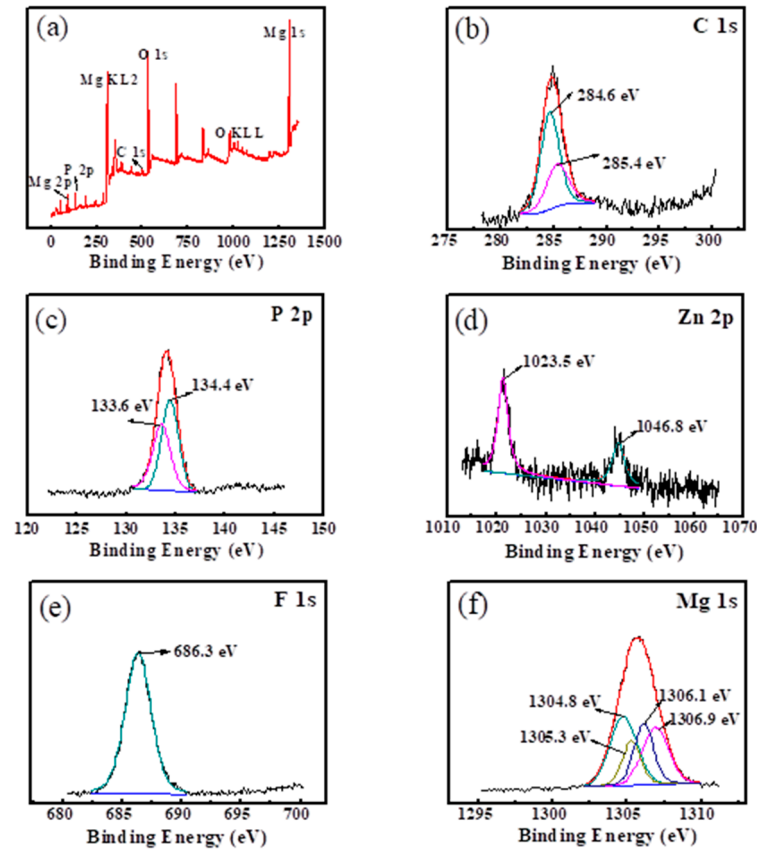


Figure 5. XPS spectra of sample No. 4: (a) survey spectrum, (b) C 1s, (c) P 2p, (d) Zn 2p, (e) F 1s, and (f) Mg 1s.

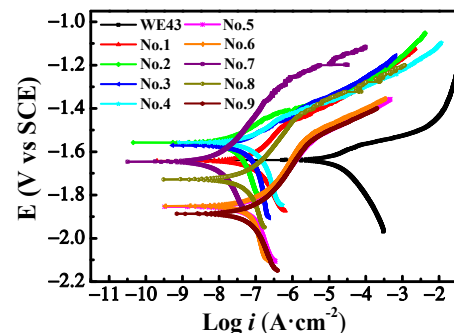


Figure 6. The potentiodynamic polarization curves measured in Hanks' solution of WE43 substrate and nine MAO samples prepared in different solutions based on the orthogonal experiment.

For the Zn amount in MAO coatings, the influencing order of four factors was ranked as EDTA-ZnNa₂ > NH₄HF₂ > H₃PO₄ > IP6. EDTA-ZnNa₂ played the most important role on affecting the Zn amount, and the increased EDTA-ZnNa₂ concentration continually improved the Zn amount in anodic coatings, indicating that Zn ions entered into anodic coatings by diffusion. NH₄HF₂ concentration was the second important processing factor affecting the Zn amount. With the increase of NH₄HF₂ concentration, the Zn amount

gradually decreased. Meanwhile, the Zn amount slightly increased with increasing H_3PO_4 concentration, which was the third important factor.

Table 2. The derived electrochemical parameters of WE43 substrate and nine treated samples prepared in different solutions based on the orthogonal experiment.

Process No.	β_a (mV/dec)	β_c (mV/dec)	i_{corr} ($A \cdot cm^{-2}$)	E_{corr} (V vs SCE)
Substrate	65.43	237.7	2.11×10^{-5}	−1.64
No. 1	248.7	343.2	1.12×10^{-7}	−1.64
No. 2	159.6	451.1	3.26×10^{-8}	−1.56
No. 3	156.5	545.6	7.01×10^{-8}	−1.57
No. 4	196.5	464.5	1.09×10^{-7}	−1.56
No. 5	164.6	523.6	8.56×10^{-8}	−1.85
No. 6	160.0	619.9	7.39×10^{-8}	−1.85
No. 7	221.2	350.9	1.09×10^{-8}	−1.65
No. 8	220.8	544.8	6.18×10^{-8}	−1.73
No. 9	183.7	439.9	8.06×10^{-8}	−1.89

Figure 7 shows the i_{corr} values, thickness; porosity; and chemical compositions, including F, P, Zn, and Mg amounts of anodic coatings fabricated on MAO samples. The i_{corr} values somewhat depend on, but not very monotonically, the thickness, porosity, or chemical composition of the MAO coatings, indicating that coating thickness, porosity, or composition was not the only important factor governing coating corrosion resistance. In other words, coating corrosion resistance was jointly determined by surface characteristics. It was clear that the P amount was negatively correlated with the F amount, indicating that P and F competed to take part in coating formation (Figure 7b). Except for samples No. 5 and No. 9, the Mg amount was also negatively correlated with the Zn amount (Figure 7b), which could be attributed to their competition to combine with PO_4^{3-} into phosphate salts.

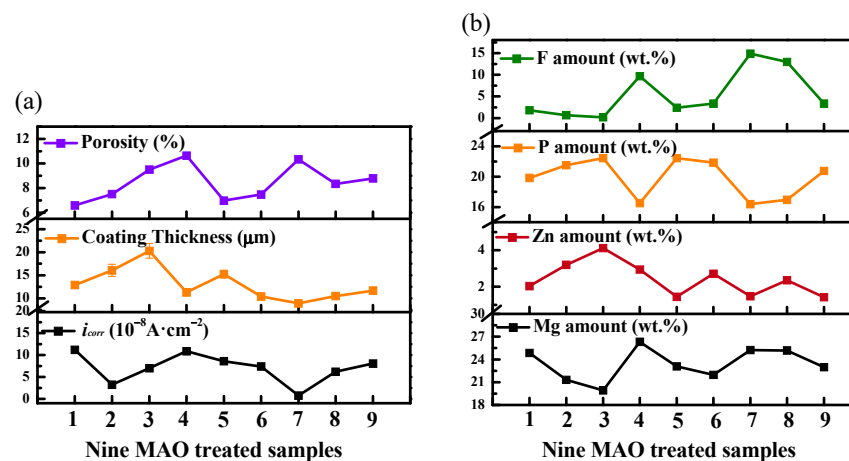


Figure 7. Correlation of i_{corr} values with thickness and porosity (a); and F, P, Zn, and Mg amounts (b) of nine anodic coatings.

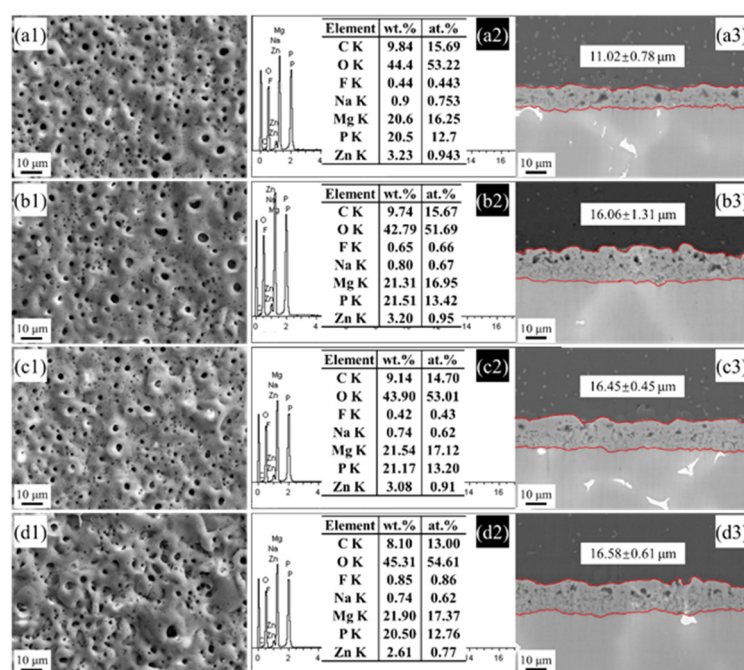
3.3. Influence of Treatment Time on Coating Property

Under constant current oxidation mode, the treatment time cannot only determine the final voltage of MAO process but also the surface characteristics and coating corrosion resistance. The prepared MAO sample in solution No. 2 achieved good corrosion resistance and a high Zn amount (3.20 wt.%). In order to clarify the influences of treatment time on the coating property, MAO samples were separately fabricated in solution No. 2 with treatment times of 2.5, 3.0, 3.5, and 4.0 min. In addition, the corresponding final voltage values under different treatment times are recorded in Table 3.

Table 3. Different treatment time and corresponding final voltage treated in No. 2 solution listed in the orthogonal experiment.

Electrolyte Constituents	Treatment Time (min)	Final Voltage (V)
No. 2 solution	2.5	484
(3 g/L NH ₄ HF ₂ , 360 g/L HMTA,	3.0	496
25 g/L H ₃ PO ₄ , 8 g/L IP6 and	3.5	506
10 g/L EDTA-ZnNa ₂)	4.0	514

Figure 8 shows surface characteristics of the anodic coatings prepared in solution No. 2 under different treatment times. According to the surface morphologies, all MAO coatings were rough with porous characteristics, and there were not any obvious differences in pore size or porosity. However, with the prolonged treatment time, the coating surface became rougher (Figure 8(a1–d1)). As shown in Figure 8(a2–d2), the prepared coatings mainly contained C, Na, F, Mg, O, Zn, and P elements. The Zn amounts in prepared anodic coatings with treatment times of 2.5, 3.0, 3.5, and 4.0 min were 3.23, 3.20, 3.08, and 2.61 wt.%, respectively, exhibiting a slightly decreased trend. According to cross-sectional morphologies shown in Figure 8(a3–d3), the thicknesses of MAO coatings prepared with treatment times of 2.5, 3.0, 3.5, and 4.0 min were 11.02 ± 0.78 , 16.06 ± 1.31 , 16.45 ± 0.45 , and 16.58 ± 0.61 μm , respectively, showing that extended treatment time could gradually increase coating thickness.

**Figure 8.** Surface morphologies (a1–d1), EDS spectra (a2–d2), and cross-sectional morphology (a3–d3) of MAO samples prepared in No. 2 solution with different treating times: (a) 2.5 min, (b) 3.0 min, (c) 3.5 min, and (d) 4.0 min.

Potentiodynamic polarization curves of treated samples in solution No. 2 with treatment times of 2.5, 3.0, 3.5, and 4.0 min are shown in Figure 9. According to the obtained corresponding electrochemical parameters listed in Table 4, with the prolongation of treatment time, the i_{corr} values slightly increased, indicating that the prolonged treatment time was unfavorable for coating corrosion resistance.

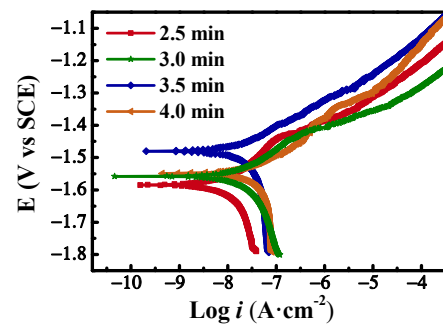


Figure 9. The measured polarization curves in Hanks' solution of MAO samples fabricated in No. 2 solution with different treatment times.

Table 4. The derived electrochemical parameters of anodic coatings prepared in No. 2 solution with treating times of 2.5, 3.0, 3.5, and 4.0 min.

Treatment Time (min)	β_a (mV/dec)	β_c (mV/dec)	i_{corr} ($A \cdot cm^{-2}$)	E_{corr} (V vs SCE)
2.5	188.8	671.7	1.65×10^{-8}	−1.58
3.0	159.6	451.1	3.26×10^{-8}	−1.56
3.5	114.2	830.1	3.49×10^{-8}	−1.48
4.0	120.6	619.6	5.18×10^{-8}	−1.55

4. Discussion

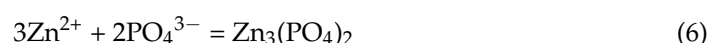
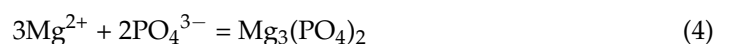
4.1. Formation Mechanism of Zn-Containing Coatings

The coating formation by MAO treatment is a complex process, which may involve some chemical reactions, such as anodization, thermal oxidation, and plasma oxidation [30]. Based on coating surface morphology, chemical composition, and phase structure, it is possible to deduce the formation mechanism of Zn-containing coatings by applying a two-stage process.

In the first stage, the used electrolytes in MAO solutions begin to ionize into corresponding ions. EDTA-ZnNa₂ can be ionized into EDTA-Zn²⁺, Na⁺, EDTA⁴⁻, and Zn²⁺ ions. Meanwhile, NH₄⁺, H⁺, and F⁻ ions are present from NH₄HF₂. Meanwhile, IP6 and EDTA⁴⁻ compete to combine with Zn²⁺ ions. In the second stage, sparks are present on the anode, the Mg sample is oxidized, and Mg²⁺ ions are developed:



At the same time, anions such as OH⁻, EDTA-Zn²⁺, PO₄³⁻, F⁻, IP6 radicals, and negatively charged zinc phytic acid complexes move toward the sample surface under the electric field between the anode and the cathode [11,31]. Meanwhile, the instantaneous temperature on the surface of the oxidized sample is very high due to spark discharge, which can hydrolyze IP6 molecules into inorganic phosphate and lower inositol phosphate (IP1-IP5) [32,33]. When these anions reach the anode surface, they combine with cations and form a stable ceramic coating under transient high temperatures and pressures. The main reaction equations on the Mg alloy surface are as follows [23]:





In this study, Zn^{2+} ions in MAO solutions exist as EDTA-Zn^{2-} or zinc phytic acid complexes, and these negatively charged Zn-containing complexes enter into MAO coatings under the electric field. EDTA-ZnNa_2 played the most important role in determining the Zn amount (Table 1). With the increase of the EDTA-ZnNa_2 concentration, the Zn amount continually increased, indicating that Zn^{2+} ions enter into anodic coatings by diffusion.

Besides OH^{-} ions, PO_4^{3-} ions and F^{-} ions can also take part in coating formation. PO_4^{3-} ions can react with both Mg^{2+} and Zn^{2+} into $\text{Mg}_3(\text{PO}_4)_2$ and $\text{Zn}_3(\text{PO}_4)_2$, while F^{-} ions combine with Mg^{2+} into MgF_2 . Because of low Zn amount in anodic coatings, $\text{Mg}_3(\text{PO}_4)_2$ may be the main phosphate. Therefore, P competes with F to take part in coating formation (Figure 7b), which could clearly explain the results that the increasing NH_4HF_2 concentration gradually decrease the Zn amount (Table 1). In addition, Mg^{2+} ions in anodic coatings can exist as MgO , $\text{Mg}_3(\text{PO}_4)_2$, or MgF_2 , while Zn^{2+} ions exist as $\text{Zn}_3(\text{PO}_4)_2$. Under some conditions, Mg^{2+} ions compete with Zn^{2+} ions to combine with PO_4^{3-} , and, therefore, the Mg amount was also negatively correlated with the Zn amount except for samples No. 5 and No. 9 (Figure 7b).

4.2. Effects of Coating Characteristics on Corrosion Resistance

For biomedical Mg alloys, the corrosion resistance of the MAO-treated sample is very important in order to achieve clinical applications. Recent results show that corrosion resistance of MAO coatings is mainly determined by chemical composition [34], micropore size or porosity [10,12], and coating thickness [12,23], while these characteristics are influenced by electrolyte composition and concentration, and electrical parameters [11].

Coating composition is an important factor in determining the corrosion resistance. It is believed that the fabricated anodic coatings composed of stable components can exhibit good corrosion resistance. In this study, Zn in MAO coatings existed as $\text{Zn}_3(\text{PO}_4)_2$, which is a very stable substance in water solution, and its solubility product constant (K_{sp}) at 298.15 K is 9.1×10^{-33} [35]. Therefore, the Zn-containing coatings achieve good corrosion resistance. However, among the nine MAO-treated samples, there are no evident differences on their Zn amounts, and, therefore, coating compositions is not an important factor in regard to corrosion resistance.

The coating thickness plays an important role on influencing the corrosion resistance. Under the same condition, thicker coatings can inhibit corrosive ions, such as chloride ions, entering into the substrate and therefore achieve better corrosion resistance [12,23]. According to Figure 7a, the i_{corr} values did not vary monotonically with coating thickness, thus indicating that coating thickness is not an important factor governing coating corrosion resistance.

Besides the coating composition and thickness, the coating micropore size or porosity can also influence the corrosion resistance of anodic coatings. Because of spark discharge, the developed MAO coatings display typically porous characteristics with some microcracks. When MAO samples are served in a corrosive environment, the defective areas provide a path for chloride ions to easily reach the substrate surface and finally result in the initiation of corrosion [36,37]. How to fabricate a uniform MAO coating with a small pore size is an important research work. According to the experimental results, the corrosion resistance is also not closely related with chemical composition, thickness, or coating porosity, thus suggesting that coating corrosion resistance is jointly determined by the coating-surface characteristics [9].

The EDTA-ZnNa_2 concentration is the first important factor in regard to coating corrosion resistance. As listed in Table 1, EDTA-ZnNa_2 at Level 2 achieved the best corrosion resistance, which can be explained based on the following two aspects. On the one hand, as our previous experimental results obtained in alkaline solutions, EDTA-ZnNa_2 was a corrosive agent of Mg alloys and therefore harmful for coating formation [15]. On the other hand, EDTA-ZnNa_2 can increase the $\text{Zn}_3(\text{PO}_4)_2$ amount and may be helpful for improving the coating corrosion resistance attributed to the highly stable characteristics

of $\text{Zn}_3(\text{PO}_4)_2$. According to the influencing regularity of EDTA- ZnNa_2 concentration on coating property, EDTA- ZnNa_2 at Level 2 achieved the best corrosion resistance.

NH_4HF_2 concentration is the second most important factor in determining the corrosion resistance of MAO coatings, and the i_{corr} values increased from Level 1 to Level 2 but decreased from Level 2 to Level 3 (Table 1). NH_4HF_2 is a widely used corrosive inhibitor of Mg alloys and is helpful for coating formation. However, with the increase of NH_4HF_2 concentration, the F amount in MAO coatings increased, and, therefore, the MgF_2 amount increased, which resulted in the decrease of the amount of $\text{Zn}_3(\text{PO}_4)_2$. Moreover, the K_{sp} of MgF_2 is 6.5×10^{-9} [38], indicating that MgF_2 is less stable compared with $\text{Zn}_3(\text{PO}_4)_2$. Therefore, the coating corrosion resistance did not exhibit a simple positive or negative relationship with the NH_4HF_2 concentration. Although the fabricated Zn-containing MAO coatings in this study exhibit excellent corrosion resistance, the Zn amount should be further increased in the future.

5. Conclusions

In near-neutral solutions, EDTA- ZnNa_2 was used as Zn source and Zn-containing MAO coatings were developed on WE43 alloys. The influences of the regularity of electrolyte compositions on corrosion resistance and the Zn content of anodic coatings were clarified by the orthogonal experiment. The order of four factors on coating corrosion resistance is EDTA- $\text{ZnNa}_2 > \text{NH}_4\text{HF}_2 > \text{IP6} > \text{H}_3\text{PO}_4$, while the sequence on the Zn amount is ranked as EDTA- $\text{ZnNa}_2 > \text{NH}_4\text{HF}_2 > \text{H}_3\text{PO}_4 > \text{IP6}$. The fabricated Zn-containing coatings achieve excellent corrosion resistance, and the lowest i_{corr} is three orders of magnitude lower than that of the WE43 substrate. The highest Zn amount of MAO coatings prepared in near-neutral solutions achieves 4.12 wt.%, and Zn ions enter into anodic coatings by diffusion. The prolonged treating time can slightly increase the coating thickness but insignificantly decrease the Zn content and corrosion resistance. In the future, the biocompatibility and antibacterial ability will be further evaluated in order to clarify in vitro biological property.

Author Contributions: Conceptualization, R.Z. (Rongfa Zhang) and R.Z. (Rongfang Zhao); software, W.L. and Y.W.; formal analysis, X.L. and Z.Y.; investigation, W.Z. and Y.Z.; data curation, S.Z.; writing—original draft preparation, W.Z. and Y.Z.; writing—review and editing, R.Z. (Rongfang Zhao) and R.Z. (Rongfa Zhang). All authors have read and agreed to the published version of the manuscript.

Funding: This study was financially supported by the National Natural Science Foundation of China (51861007, 52061013, and 51661010) and Open Fund of Material Corrosion and Protection Key Laboratory of Sichuan Province (No. 2021CL28).

Institutional Review Board Statement: Not applicable.

Informed Consent Statement: Not applicable.

Data Availability Statement: Not applicable.

Conflicts of Interest: The authors declare no conflict of interest.

References

1. Jamari, J.; Ammarullah, M.I.; Santoso, G.; Sugiharto, G.; Supriyono, T.; van der Heide, E. In Silico Contact Pressure of Metal-on-Metal Total Hip Implant with Different Materials Subjected to Gait Loading. *Metals* **2022**, *12*, 1241. [[CrossRef](#)]
2. Li, X.; Liu, X.; Wu, S.; Yeung, K.W.K.; Zheng, Y.; Chu, P.K. Design of magnesium alloys with controllable degradation for biomedical implants: From bulk to surface. *Acta Biomater.* **2016**, *45*, 2–30. [[CrossRef](#)] [[PubMed](#)]
3. Brooks, E.; Ehrensberger, M. Bio-corrosion of magnesium alloys for orthopaedic applications. *J. Funct. Biomater.* **2017**, *8*, 38. [[CrossRef](#)] [[PubMed](#)]
4. Liao, J.; Hotta, M. Corrosion products of field-exposed Mg-Al series magnesium alloys. *Corros. Sci.* **2016**, *112*, 276–288. [[CrossRef](#)]
5. Li, L.; Zhang, M.; Li, Y.; Zhao, J.; Qin, L.; Lai, Y. Corrosion and biocompatibility improvement of magnesium-based alloys as bone implant materials: A review. *Regen. Biomater.* **2017**, *4*, 129–137. [[CrossRef](#)]
6. Li, X.J.; Zhang, M.; Wen, S.; Mao, X.; Huo, W.G.; Guo, Y.Y.; Wang, Y.X. Microstructure and wear resistance of micro-arc oxidation ceramic coatings prepared on 2A50 aluminum alloys. *Surf. Coat. Technol.* **2020**, *394*, 125853. [[CrossRef](#)]

7. Cheng, Y.L.; Feng, T.; Cheng, Y.L. A systematic study of the role of cathodic polarization and new findings on the soft sparking phenomenon from plasma electrolytic oxidation of an Al-Cu-Li alloy. *J. Electrochem. Soc.* **2022**, *163*, 071505. [[CrossRef](#)]
8. Yao, Z.P.; Li, L.L.; Jiang, Z.H. Adjustment of the ratio of Ca/P in the ceramic coating on Mg alloy by plasma electrolytic oxidation. *Appl. Surf. Sci.* **2009**, *255*, 6724–6728. [[CrossRef](#)]
9. Dou, J.; Gu, G.; Chen, C.; Pan, Y. Characterization and biodegradation behavior of micro-arc oxidation coatings formed on Mg-Zn-Ca alloys in two different electrolytes. *RSC Adv.* **2016**, *6*, 1488–14818. [[CrossRef](#)]
10. Wen, C.; Zhan, X.; Huang, X.; Xu, F.; Luo, L.; Xia, C. Characterization and corrosion properties of hydroxyapatite/graphene oxide bio-composite coating on magnesium alloy by one-step micro-arc oxidation method. *Surf. Coat. Technol.* **2017**, *317*, 125–133. [[CrossRef](#)]
11. Zhang, R.F.; Shan, D.Y.; Chen, R.S.; Han, E.H. Effects of electric parameters on properties of anodic coatings formed on magnesium alloys. *Mater. Chem. Phys.* **2008**, *107*, 356–363. [[CrossRef](#)]
12. Liu, S.; Li, Z.; Yu, Q.; Qi, Y.; Peng, Z.; Liang, J. Dual self-healing composite coating on magnesium alloys for corrosion protection. *Chem. Eng. J.* **2021**, *424*, 130551. [[CrossRef](#)]
13. Xu, L.Y.; Zhang, D.J.; Su, H.J.; Yu, P.; Wan, Y.; Sun, H.L. Improving the tribocorrosion performance of plasma electrolytic oxidized coatings on AZ31B magnesium alloy using pullulan as an electrolyte additive. *Surf. Coat. Technol.* **2022**, *446*, 128754. [[CrossRef](#)]
14. Zhao, Q.M.; Li, G.Z.; Zhu, H.M. Preparation and performance characterization of bioactive coating on magnesium alloy. *J. Biobased Mater. Bio.* **2017**, *11*, 473–476. [[CrossRef](#)]
15. Zhu, Y.Y.; Zhang, S.F.; Zhao, R.F.; Lou, J.; Zhang, R.F.; Huan, X.X.; Zhang, Y.J. Influences of Na₂SiO₃ and EDTA-ZnNa₂ concentration on properties of zinc-containing coatings on WE43 magnesium alloys. *Surf. Coat. Technol.* **2018**, *356*, 108–122. [[CrossRef](#)]
16. dos Santos, A.P.; Muhaffel, F.; Paksoy, A.H.; Cimenoglu, H. Production of a coating containing Ca, P and Zn on AZ31 magnesium alloy by micro arc oxidation. In Proceedings of the International Scientific Conference, Gabrovo, Bulgaria, 18–19 November 2016.
17. Fraga, C.G. Relevance, essentiality and toxicity of trace elements in human health. *Mol. Asp. Med.* **2005**, *26*, 235–244. [[CrossRef](#)] [[PubMed](#)]
18. Song, Y.; Leonard, S.W.; Traber, M.G.; Ho, E. Zinc Deficiency Affects DNA Damage, Oxidative Stress, Antioxidant Defenses, and DNA Repair in Rats. *J. Nutr.* **2009**, *139*, 1626–1631. [[CrossRef](#)]
19. Tapiero, H.; Tew, K.D. Trace elements in human physiology and pathology: Zinc and metallothioneins. *Biomed. Pharmacother.* **2003**, *57*, 399–411. [[CrossRef](#)]
20. Lonergan, Z.R.; Nairn, B.L.; Wang, J.; Hsu, Y.; Hesse, L.E.; Beavers, W.N.; Chazin, W.J.; Trinidad, J.C.; van Nieuwenhze, M.S.; Giedroc, D.P.; et al. An *Acinetobacter baumannii*, Zinc-Regulated Peptidase Maintains Cell Wall Integrity during Immune-Mediated Nutrient Sequestration. *Cell Rep.* **2019**, *26*, 2009–2018. [[CrossRef](#)]
21. Mori, Y.; Koshi, A.; Liao, J.; Asoh, H.; Ono, S. Characteristics and corrosion resistance of plasma electrolytic oxidation coatings on AZ31B Mg alloy formed in phosphate—Silicate mixture electrolytes. *Corros. Sci.* **2014**, *88*, 254–262. [[CrossRef](#)]
22. Shi, X.T.; Wang, Y.; Li, H.Y.; Zhang, S.F.; Zhao, R.F.; Li, G.Q.; Zhang, R.F.; Sheng, Y.; Cao, S.Y.; Zhao, Y.J.; et al. Corrosion resistance and biocompatibility of calcium-containing coatings developed in near-neutral solutions containing phytic acid and phosphoric acid on AZ31B alloy. *J. Alloys Compd.* **2020**, *823*, 153721. [[CrossRef](#)]
23. Lin, Z.S.; Wang, T.L.; Yu, X.M.; Sun, X.T.; Yang, H.Z. Functionalization treatment of micro-arc oxidation coatings on magnesium alloys: A review. *J. Alloys Compd.* **2021**, *879*, 160453. [[CrossRef](#)]
24. Xu, J.L.; Tao, S.C.; Ba, L.Z.; Luo, J.M.; Zheng, Y.F. Effects of Mo contents on the microstructure, properties and cytocompatibility of the microwave sintered porous Ti-Mo alloys. *Mater. Sci. Eng.* **2019**, *97*, 156–165. [[CrossRef](#)] [[PubMed](#)]
25. Li, J.Y.; Shi, H.W.; Liu, F.C.; Han, E.H. Self-healing epoxy coating based on tung oil-containing microcapsules for corrosion protection. *Prog. Org. Coat.* **2021**, *158*, 106236. [[CrossRef](#)]
26. Zhang, R.F.; Zhang, S.F.; Xiang, J.H.; Zhang, L.H.; Zhang, Y.Q.; Guo, S.B. Influence of sodium silicate concentration on properties of micro arc oxidation coatings formed on AZ91HP magnesium alloys. *Surf. Coat. Technol.* **2012**, *206*, 5072–5076. [[CrossRef](#)]
27. Liu, J.; Zhu, R.L.; Xu, T.Y.; Xu, Y.; Ge, F.; Xi, Y.F.; Zhu, J.X.; He, H.P. Co-adsorption of phosphate and zinc (II) on the surface of ferrihydrite. *Chemosphere* **2016**, *144*, 1148–1155. [[CrossRef](#)]
28. Jin, G.D.; Cao, H.L.; Qiao, Y.Q.; Meng, F.H.; Zhu, H.Q.; Liu, X.Y. Osteogenic activity and antibacterial effect of zinc ion implanted titanium. *Colloids Surf.* **2014**, *117*, 158–165. [[CrossRef](#)]
29. Jia, Z.J.; Li, M.; Liu, Q.; Xu, X.C.; Cheng, Y.; Zheng, Y.F.; Xi, T.F.; Wei, S.C. Micro-arc oxidization of a novel Mg-1Ca alloy in three alkaline KF electrolytes: Corrosion resistance and cytotoxicity. *Appl. Surf. Sci.* **2014**, *292*, 1030–1039. [[CrossRef](#)]
30. Cui, X.J.; Liu, C.H.; Yang, R.S.; Li, M.T.; Lin, X.Z. Self-sealing micro-arc oxidation coating on AZ91D Mg alloy and its formation mechanism. *Surf. Coat. Technol.* **2015**, *269*, 228–237. [[CrossRef](#)]
31. Qiao, L.P.; Lou, J.; Zhang, S.F.; Qu, B.; Chang, W.H.; Zhang, R.F. The entrance mechanism of calcium and phosphorus elements into micro arc oxidation coatings developed on Ti6Al4V alloy. *Surf. Coat. Technol.* **2016**, *285*, 187–196. [[CrossRef](#)]
32. Lee, K.M.; Shin, K.R.; Namgung, S.; Yoo, B.; Shin, D.H. Electrochemical response of ZrO₂-incorporated oxide layer on AZ91 Mg alloy processed by plasma electrolytic oxidation. *Surf. Coat. Technol.* **2011**, *205*, 3779–3784. [[CrossRef](#)]
33. Zhang, R.Y.; Cai, S.; Xu, G.H.; Zhao, H.; Li, Y.; Wang, X.X.; Huang, K.; Ren, M.G.; Wu, X.D. Crack self-healing of phytic acid conversion coating on AZ31 magnesium alloy by heat treatment and the corrosion resistance. *Appl. Surf. Sci.* **2014**, *313*, 896–904. [[CrossRef](#)]

34. Liang, J.; Srinivasan, P.B.; Blawert, C.; Dietzel, W. Comparison of electrochemical corrosion behaviour of MgO and ZrO₂ coatings on AM50 magnesium alloy formed by plasma electrolytic oxidation. *Corros. Sci.* **2009**, *51*, 2483–2492. [[CrossRef](#)]
35. Zhou, X.M.; Bai, H.L.; Ma, H.; Li, H.B.; Yuan, W.X.; Du, H.J.; Zhang, P.X.; Xin, H. Synthesis of zinc phosphate and zinc ammonium phosphate nanostructures with different morphologies through pH control. *Mater. Character.* **2015**, *108*, 22–28. [[CrossRef](#)]
36. Ma, H.J.; Gu, Y.H.; Liu, S.J.; Che, J.T.; Yang, D.W. Local corrosion behavior and model of micro-arc oxidation HA coating on AZ31 magnesium alloy. *Surf. Coat. Technol.* **2017**, *331*, 179–188. [[CrossRef](#)]
37. Chen, J.F.; Lin, W.X.; Liang, S.Y.; Zou, L.Z.; Wang, C.; Wang, B.S.; Yan, M.F.; Cui, X.P. Effect of alloy cations on corrosion resistance of LDH/MAO coating on magnesium alloy. *Appl. Surf. Sci.* **2019**, *463*, 535–544. [[CrossRef](#)]
38. Teaching and Research Group of Inorganic Chemistry at Northeastern University. *University Chemistry (I)*; Northeast University Press: Shenyang, China, 1993; p. 402. (In Chinese)